Journal of Hazardous Materials 443 (2023) 130224

Contents lists available at ScienceDirect

Journal of Hazardous Materials

journal homepage: www.elsevier.com/locate/jhazmat

Research Article

Periodic mesoporous organosilicas containing naphthalenediimides as organic sensitizers for sulfadiazine photodegradation

Bruna Castanheira [a,*], Sergio Brochsztain [b], Larissa Otubo [c], Antonio Carlos S.C. Teixeira [a,*]

[a] Department of Chemical Engineering, University of São Paulo, Av. Prof. Luciano Gualberto, tr. 3, São Paulo 380, SP, Brazil
[b] Federal University of ABC, Av. dos Estados, 5001, Santo André, SP 09210-580, Brazil
[c] Nuclear and Energy Research Institute (IPEN), Av. Prof. Lineu Prestes, 2242, São Paulo, SP 05508-000, Brazil

HIGHLIGHTS

- PMOs functionalized with naphthalenediimides (NDI) are efficient photocatalysts.
- The potential of PMONDI to degrade an antibiotic (sulfadiazine) was demonstrated.
- Sulfadiazine can be degraded by $^1O_2$ and triplet naphthalenediimide (^{3}NDI*).
- PMONDI performed better than TiO_2 supported on SBA-15 mesoporous silica.
- The stability of the PMONDI photocatalysts was demonstrated by reuse tests.

GRAPHICAL ABSTRACT

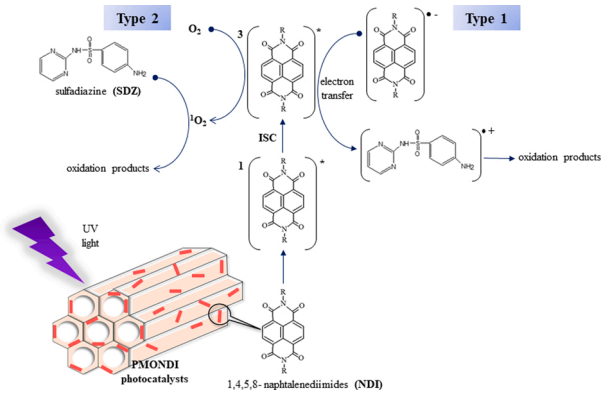

ARTICLE INFO

Editor: Dr. C. Baiyang

Keywords:
Periodic Mesoporous Organosilicas
Naphthalenediimides
Contaminants of Emerging Concern
Sulfadiazine
Heterogeneous Photocatalysis

ABSTRACT

In this work, periodic mesoporous organosilicas (PMO) functionalized with the organic sentisizer naphthalenediimide (NDI) were employed as heterogeneous catalysts for the photodegradation of the antibiotic sulfadiazine (SDZ), taken as a model for contaminants of emerging concern (CECs). The catalysts, designated as PMONDI, were prepared by surfactant-directed co-condensation of the precursor N,N′-bis(3-triethoxysilylpropyl)– 1,4,5,8-naphthalenediimide with tetraethoxysilane. The synthesized PMONDI were characterized using transmission electron microscopy, nitrogen adsorption isotherms and small and large angle x-ray scattering. The performance of PMONDI catalysts in the photodegradation of SDZ was compared to that of TiO_2 nanoparticles impregnated into SBA-15 mesoporous silica (TiO_2/SBA-15), under irradiation with a Hg lamp with a bandpass filter of 320–500 nm. Under optimal conditions, PMONDI degraded 100% of the SDZ in 45 min, while the total degradation of SDZ was achieved only after 150 min with TiO_2/SBA-15. PMONDI also performed better than TiO_2/SBA-15 in reuse tests. The mechanism of photodegradation with PMONDI involves the formation of excited triplet states of NDI (^{3}NDI*) upon irradiation, which can then react with molecular oxygen to form reactive oxygen species, which degrade SDZ. Analysis of the SDZ degradation products indicated two main pathways: (1) hydroxylation of the aniline ring and (2) SO_2 extrusion and rearrangement, followed by oxidation

* Corresponding authors.
E-mail addresses: brucastan@gmail.com (B. Castanheira), acscteix@usp.br (A.C.S.C. Teixeira).

https://doi.org/10.1016/j.jhazmat.2022.130224
Received 6 July 2022; Received in revised form 27 September 2022; Accepted 19 October 2022
Available online 20 October 2022

of the aniline ring to nitrobenzene. In conclusion, the great potential of the PMONDI materials as photocatalysts for CECs degradation was demonstrated in this work, encouraging further research on these materials for the degradation of pollutants.

1. Introduction

Contaminants of emerging concern (CECs), such as pharmaceutical active compounds, synthetical and natural hormones, pesticides, personal care products and food additives, have been continuously introduced in the environment by anthropogenic sources in the last decades (Rivera-Utrilla et al., 2013; Tijani et al., 2016; Rodriguez-Narvaez et al., 2017; Ahmed et al., 2017; Krzeminski et al., 2019; Rizzo et al., 2019; Parida et al., 2021). Consequently, CECs have been frequently detected in rivers, lakes and reservoirs at the ng L^{-1} to μg L^{-1} levels, or even higher. In spite of the risks CECs pose to the environment and human health, they are in general not monitored and there is no regulation for their control in most countries (Rivera-Utrilla et al., 2013; Tijani et al., 2016; Rodriguez-Narvaez et al., 2017; Ahmed et al., 2017; Krzeminski et al., 2019; Rizzo et al., 2019; Parida et al., 2021). The presence of antibiotics in the environment is particularly concerning, since they can induce bacterial resistance and can also interfere with the metabolism of fish and other living beings (Kümmerer, 2009a, 2009b; Kovalakova et al., 2020). Among antibiotics, sulfonamides, such as sulfadiazine (SDZ, Fig. 1), are of special interest, because of their wide veterinary use in the prevention of diseases in livestock (Baran et al., 2011). Most of the administered dose of SDZ (90%) is not absorbed by the living organisms, and is excreted unmodified into the environment. SDZ is highly soluble in water, and therefore accumulates in water bodies.

Most CECs are not removed in conventional urban wastewater treatment plants. Therefore, there has been a renewed interest in methods for degrading/inactivating CECs. Among the different methods, advanced oxidation processes (AOPs), consisting in the photocatalytic degradation of the pollutant in the presence of heterogeneous catalysts, have attracted extensive attention in the past few decades (Miklos et al., 2018; Lee et al., 2021). Several studies have shown that SDZ and other sulfonamides are susceptible to photocatalytic degradation by AOPs (Zessel et al., 2014; Rivas-Ortiz et al., 2017; Yang et al., 2017). Titanium dioxide (TiO_2) nanoparticles have been by far the most used photocatalyst in AOPs (Miranda-García et al., 2014; Fagan et al., 2016). TiO_2 nanoparticles, however, show a strong tendency to agglomerate in aqueous media. A solution to overcame this drawback, adopted by several authors, is the dispersion of TiO_2 nanoparticles in mesoporous silicas, such as SBA-15 (Fig. 2A), which features well-organized pores with diameter in the range of 8–12 nm (Lopez-Munoz et al., 2005; Yang et al., 2006; Acosta-Silva et al., 2011; Salameh et al., 2015; Conceição et al., 2017; Castanheira et al., 2022). Furthermore, the organized 1D pore system in mesoporous silicas provides a confined environment, working as a nanoreactor for photoinduced reactions. In addition, mesoporous silicas can be post-synthetically functionalized with organic groups, which can act as sensitizers in the photodegradation of pollutants, as an alternative to inorganic sensitizers such as TiO_2 (Castanheira et al., 2017).

Post-synthetic functionalization of mesoporous silicas, however, often leads to pore blockage. In this context, periodic mesoporous organosilicas (PMOs) (Hoffmann et al., 2006; Mizoshita et al., 2011; Van Der Voort et al., 2013; Park et al., 2014; Karimi et al., 2022) are very attractive materials to support sensitizers in the photocatalytic removal of CECs. PMOs are hybrid materials synthesized by a surfactant-templated method, using bis-silylated bridging organosilanes of the type $(RO)_3Si-R'-Si(OR)_3$ as silica sources (Fig. 2B). As a result, the organic moiety is incorporated as an integral part of the pore walls, leaving the pore voids unblocked, in contrast to post-synthetic grafting, where the organic groups adhere to the interior of the pores. Thanks to those qualities, PMOs have recently found important environmental applications, including pollutant removal by adsorption and photocatalysis (Esquivel et al., 2017; Deka et al., 2014; Chongdar et al., 2022).

In the present work, we demonstrate that PMOs functionalized with naphthalenediimides (NDI) as organic sensitizers are quite efficient materials for the photodegradation of SDZ. The synthesis of these materials, which were named PMONDI, has been recently accomplished by our group (Castanheira et al., 2018; Andrade et al., 2020; Moraes et al., 2018). They are synthesized by the co-condensation of tetraethoxysilane (TEOS) with N,N′-bis(3-triethoxysilylpropyl)−1,4,5,8-naphthalenediimide (TESP-NDI), a NDI-based bridged silsesquioxane, in the presence of the surfactant Pluronics P123 as a template (Fig. 2B). NDI (Fig. 1) are *n*-type organic semiconductors with a variety of applications, such as in solar cells, light emitting diodes, photochromic devices and photocatalysis (Kumar et al., 2018; Bhosale et al., 2021). NDI derivatives, when irradiated, form triplet states that readily react with molecular oxygen, generating singlet oxygen ($^1O_2$), which can then degrade different organic substrates (Type II photodegradation mechanism) (Aveline et al., 1997; Rogers and Kelly, 1999). Triplet excited states of NDI can also accept electrons from the pollutant molecules, generating reactive species, leading to further degradation (Type I photodegradation mechanism) (Kumar et al., 2018; Bhosale et al., 2021; Aveline et al., 1997; Rogers and Kelly, 1999).

In this work, the photocatalytic activity of PMONDI was compared with that of a mesoporous silica SBA-15 impregnated with TiO_2. This material, containing 16% (w/w) TiO_2, was named 16% TiO_2/SBA-15, and prepared by post-synthetic modification of pristine SBA-15 (Fig. 2A). It was designed to have the same active photocatalytic material content as the PMONDI-16 sample, which contains 16% (w/w) NDI. We show that the PMONDI photocatalysts perform better than the TiO_2-based catalyst for SDZ degradation under similar irradiation conditions.

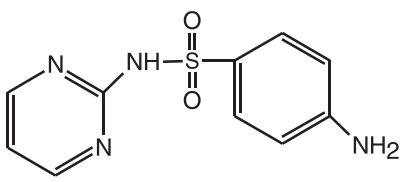

Sulfadiazine (SDZ)

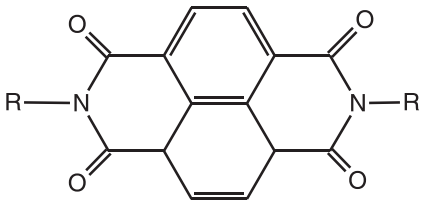

Naphtalenediimide (NDI)

Fig. 1. Structures of the antibiotic sulfadiazine, used here as a CEC model, and of the naphthalenediimide photosensitizer.

2. Experimental part

2.1. Materials

Sulfadiazine (99% purity) and titanium (IV) isopropoxide (TTIP, 97% purity) were obtained from Sigma-Aldrich. Ethanol and acetic acid (HPLC grade) were purchased from Baker. Furfuryl alcohol (FFA) was obtained from TCI America. All solutions used throughout this study were prepared with deionized water. Pristine SBA-15 was prepared according to a standard literature procedure (Zhao et al., 1998) 16% TiO_2/SBA-15 was prepared via sol-gel hydrolysis and condensation of an isopropanol solution of TTIP in the presence of pre-synthesized SBA-15 silica support (Fig. 2A), according to reported methods (Lopez-Munoz et al., 2005; Yang et al., 2006; Acosta-Silva et al., 2011; Salameh et al., 2015; Conceição et al., 2017). The detailed procedure is given in the Supplementary Information.

The PMONDI photocatalysts were synthesized and characterized as previously reported (Castanheira et al., 2018). Briefly, the precursor TESP-NDI (Fig. 2B) was synthesized by the reaction between 1,4,5,8-naphthalenetetracarboxylic dianhydride and 3-aminopropyltriethoxysilane. Co-condensation of TESP-NDI with tetraethoxysilane (TEOS) in acidic media, in the presence of the surfactant Pluronic P123 as a template, resulted in the formation of the PMONDI (Fig. 2B), containing variable amounts of the NDI sensitizer. The samples employed here contained either 8 wt% NDI (PMONDI-8) (molar ratio = 82 SiO_2: 1 NDI) or 16 wt% NDI (PMONDI-16) (molar ratio = 38 SiO_2: 1 NDI). The NDI contents were calculated from elemental analysis (more details are given elsewhere) (Castanheira et al., 2018).

2.2. Characterization of the photocatalysts

High resolution transmission electron microscopy (HRTEM) images were obtained with a JEOL JEM 2100 microscope operating at 200 kV. N_2 adsorption-desorption isotherms were measured at 77 K using a Nova 2200 Surface Area and Pore Size Analyzer (Quantachrome). The surface areas were obtained by the Brunauer-Emmett-Teller (BET) method. Pore volumes were calculated at $P/P_0 = 0.97$. Pore diameters were obtained by the Barrett-Joyner-Halenda (BJH) method (desorption branch). Diffuse reflectance spectroscopy (DRS) was performed with a Cary 50 UV–visible spectrophotometer, using an external optical fiber accessory (Barrelino).

Small angle X-ray scattering measurements (SAXS) were carried out using a Xeuss 2.0 equipment, equipped with a generating source Xenocs with CuKα (λ = 0.15406 nm) radiation. All the samples were scanned under the same conditions in the range 2θ = 0–3°. The hexagonal cell parameter (a_0) was determined according to Eq. (1):

$$a_0 = \frac{2d_{100}}{\sqrt{3}} \quad (1)$$

Where d_{100} corresponds to the Bragg's distance reflection at the (100) crystallographic plane. In addition, the TiO_2 nanocrystals present on the TiO_2/SBA-15 materials were characterized with wide-angle XRD patterns recorded on a Bruker (D8-Discover) powder X-ray diffractometer using CuKα radiation (40 KV, 30 mA), LynxEye detector and Ni filter in the 2θ range 10°−100° with a scanning rate of 0.75° min^{-1}. From the line broadening of the corresponding X-ray diffraction peaks, the TiO_2 crystallite size was estimated using the Scherrer equation (Eq. 2), where L is the average crystallite size in nm, λ is the wavelength of X-ray radiation (CuKα = 0.154056 nm), K is shape factor, taken as 0.9, β is the broadened profile width at half maximum height in radians and θ is the diffracting angle.

$$L = \frac{K\lambda}{\beta cos\theta} \quad (2)$$

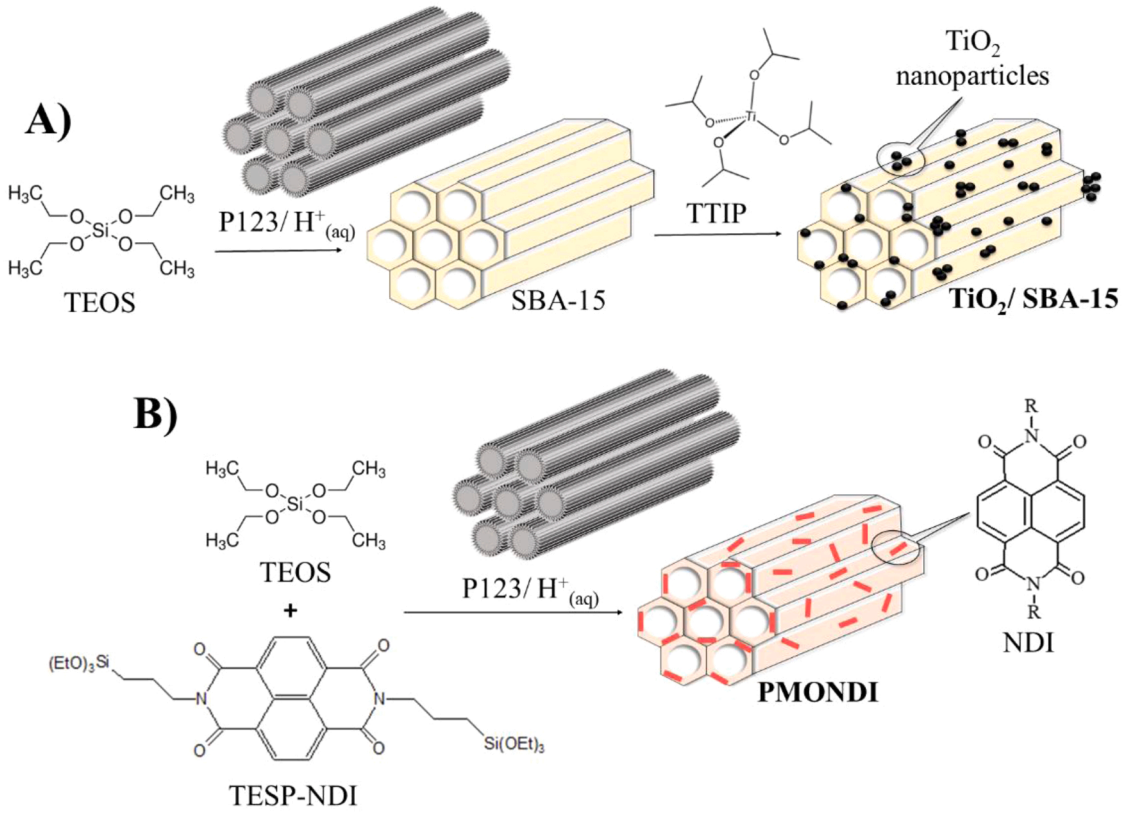

Fig. 2. Schematic representation of the synthesis and structure of (A) TiO_2/SBA-15 and (B) PMONDI. TEOS = tetraethoxysilane; P123 = Pluronics P123 (surfactant); TTIP = titanium tetraisopropoxide; TESP-NDI = N,N′-bis(3-triethoxysilylpropyl)−1,4,5,8-naphthalenediimide.

2.3. Irradiation experiments

Photocatalytic reactions were carried out in a jacketed beaker as a batch reactor (Fig. 3). The temperature was kept constant at 25 °C by recirculating water through a thermostatic bath. The pH of the solutions was not controlled, and remained close to 7.0 during the experiments. The photocatalyst suspensions in SDZ solution were stirred for 24 h in the dark before irradiation, in order to establish the adsorption/desorption equilibrium between SDZ and the surface of the catalysts. The irradiation was performed using an Omnicure S1000 Hg lamp (100 W, bandpass filter: 320–500 nm), containing an optic fiber guide. The irradiance spectrum of the lamp (Fig. S1) was registered using a Luzchem SPR-02 spectroradiometer. The distance between the tip of the optic fiber and the solution was 15 cm, and the surface area of irradiated liquid was 36.3 cm^2 (Fig. 3).

In a typical run, 25 mg of catalyst was dispersed in 50 mL of SDZ solution. The initial concentration of SDZ and the lamp intensity were varied in each run, according to Table 1. Initial SDZ concentrations were established based on wastewater from pharmaceutical production and formulation facilities, where contaminants of environmental concern can be found at concentrations at the low level of mg L^{-1} (Parida et al., 2021; Kümmerer, 2009a, 2009b; Kovalakova et al., 2020; Baran et al., 2011). Furthermore, this choice allows direct quantification of the analyte by liquid chromatography, without the need for pre-concentration steps, avoiding the introduction of additional variability in the data.

During irradiation, aliquots of 0.5 mL were taken at 15 min intervals from the irradiated solution, filtered through a 0.45 μm membrane filter and analyzed by HPLC. Control experiments, such as photolysis and irradiation with non-functionalized mesoporous silica (SBA-15), were also carried out under the conditions in Table 1. The experimental error and the standard deviation of the experiment performed in triplicate (central point conditions) were considered equal for all experiments.

Pseudo-first-order kinetic constants (k_{SDZ}, min^{-1}) for the decay of [SDZ] with time were calculated by Eq. 2, where [SDZ] and $[SDZ]_0$ are the concentrations of SDZ at time t and $t = 0$, respectively.

$$[SDZ] = [SDZ]_0 \times e^{-k_{SDZ}t} \quad (3)$$

The reusability of PMONDI-16% and 16% TiO_2/SBA-15 catalysts was evaluated over three consecutive cycles using the conditions of experiment B (Table 1). At the end of each cycle, the spent catalyst was filtered off and oven-dried for 24 h (50 °C) before being used for the next run, with a fresh SDZ solution.

Table 1
Initial SDZ concentrations and irradiances used in the experiments.

Experiment	I (mW cm^{-2})	$[SDZ]_0$ (mg L^{-1})
A	3	7.5
B	3	12.5
C	8	5
D[a]	8	10
E	8	15
F	13	7.5
G	13	12.5

[a] performed in triplicate.

2.4. Quantification of singlet oxygen species

The $^1O_2$ at steady state concentration ($[^1O_2]_{SS}$) was measured using FFA as probe. For this, the same amount of the PMONDI-16 used in the irradiation tests (25 mg) were dispersed in 50 mL of FFA at an initial concentration of 10^{-4} mol L^{-1}. The suspension was stirred during 24 h at 25 °C to guarantee adsorption of the probe solution onto photocatalytic materials. The light source was set at I = 12.5 mW cm^{-2} and turned on. Aliquots of 1 mL of the aqueous suspension were collected from the reactor and filtered through a 0.45-μm membrane filter to remove the catalyst powder and stored at freezer for HPLC analysis.

The reaction between FFA and $^1O_2$ is controlled by diffusion according to the following equation: (Mostafa and Rosario-Ortiz, 2013)

$$\frac{-d[FFA]}{dt} = k_{1O2,FFA}[1O2]ss \quad [FFA] \quad (4)$$

where, $[^1O_2]$ and [FFA] are the concentrations of $^1O_2$ and FFA, respectively and $k_{1O2,FFA} = 1.2 \times 10^{-8}$ L mol^{-1} s^{-1} is the second order rate constant of the reaction between $^1O_2$ and FFA.

If the illumination intensity is constant and the FFA concentration is sufficiently low ($\leqq 2 \times 10^{-4}$ mol L^{-1}), the steady-state concentration of $^1O_2$ can be calculated from the following equations:

$$\frac{-d[FFA]}{dt} = k_{obs}[FFA] \quad (5)$$

$$[1O2]ss = \frac{k_{obs}}{k_{1O2,FFA}} \quad (6)$$

where k_{obs} corresponds to the observed specific pseudo-first order degradation rate of FFA.

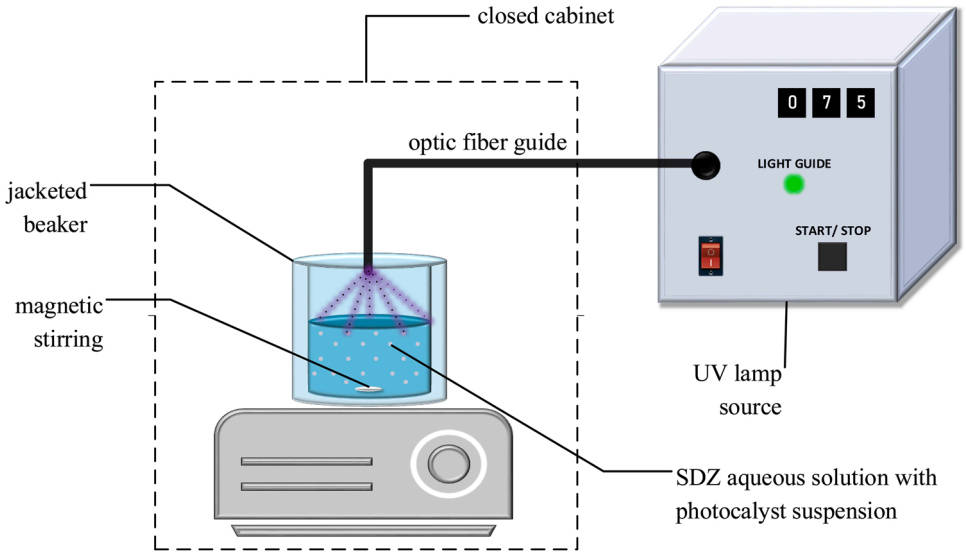

Fig. 3. Experimental arrangement for the irradiation studies.

2.5. Detection of SDZ, FFA and degradation products

SDZ and FFA concentrations were monitored by ultra-fast liquid chromatography, using a Shimadzu LC 20 CE chromatograph, equipped with a C18 column (Phenomenex Synergy Fusion-RP 80 A, 150 mm × 4.60 mm, 4 μm) and a UV–visible detector (SPD 20 A). SDZ was determined at 266 nm by an isocratic elution with 80% acetic acid (1%) and 20% acetonitrile, FFA was monitored at 234 nm using 50% methanol and 50% acetic acid as mobile phase. The oven temperature, sample injection volume and flow rate were 40 °C, 50 μL e 1 mL min^{-1}, respectively for all the methods. Under these conditions, the limits of detection and quantification were 0.03 mg L^{-1} and 0.09 mg L^{-1} for SDZ and 0.01 mg L^{-1} and 0.05 mg L^{-1} for FFA, respectively.

Degradation products of SDZ formed during irradiation were analyzed with a Shimadzu LCMS-IT-TOF High Speed Liquid Chromatograph - Mass Spectrometer (LC-20 CE with an electrospray ionization source), employing the same column, injection volume and eluents as described above, and flow rate of 0.3 mL min^{-1}. The mass-spectral data were obtained in positive mode between m/z 50 and 500 and the operating conditions were as follows: 11 L min^{-1} for desolvating gas flow; source and desolvation temperatures: 200 °C both; capillary voltage: 4.50 kV. The collision energy (CE) was held at 50% for MS analysis; the collision gas applied was argon (> 99.99% purity). The error between experimental and calculated m/z ratios was less than 1 mg L^{-1} for all identified compounds.

3. Results and discussion

3.1. Characterization of the photocatalysts

HRTEM images of pristine SBA-15, 16% TiO_2/SBA-15 and PMONDI-16 are shown in Fig. 4. The presence of organized parallel mesochannels is evident in all the materials. The modified SBA-15 materials, however, presented less organized pore structures than pristine SBA-15 (Fig. 4A), as well as smaller grain sizes. TiO_2 nanoparticles of 5–10 nm size are clearly seen attached to the SBA-15 grains in the 16% TiO_2/SBA-15 material (Fig. 4B). Some of the nanoparticles seem to be inside the mesopores, although this fact cannot be ascertained. In the case of PMONDI-16, wide pores can be seen in the image (Fig. 4C), in agreement with the placement of the NDI units within the pore walls, leaving a large void space suitable for the catalytic activity.

All catalyst samples presented SAXS patterns consistent with a 2D-hexagonal mesoscopic structure, typical of SBA-15 type materials (Fig. S2A). The N_2 adsorption isotherms are shown in Fig. S2B, which are typically of the type IV(a) with H1 hysteresis loop, which also are typical of 2D-hexagonal SBA-15 materials (Zhao et al., 1998). The corresponding textural parameters are shown in Table 2. Note that the specific surface area (S_{BET}), pore volume (V_p) and pore diameter of 16% TiO_2/SBA-15 were nearly unchanged as compared to pristine SBA-15, indicating that the TiO_2 NP were deposited on the external surface of the SBA-15 grains, in agreement with the TEM image (Fig. 4B). In the case of the PMONDI, on the other hand, a decrease in S_{BET} and V_p was observed at high organic loadings, although the pore diameter increased, since the NDI precursor acts as a micelle swelling agent during PMO synthesis (Castanheira et al., 2018). The large pore sizes presented by the PMONDI catalysts can favor the mass transfer into the pores, so enhancing the photocatalytic activity.

The XRD of 16% TiO_2/SBA-15 (Fig. S2C) confirmed the presence of TiO_2 in the anatase form. The average crystallite size was determined by

Table 2
Textural parameters of the catalysts studied.

Catalyst	S_{BET} (cm^2 g^{-1})	V_p (cm^3 g^{-1})	Pore size (nm)
SBA-15	594	0.87	5.2
16% TiO_2/SBA-15	592	0.78	5.2
PMONDI-8	562	1.08	12.6
PMONDI-16	441	0.64	10.2

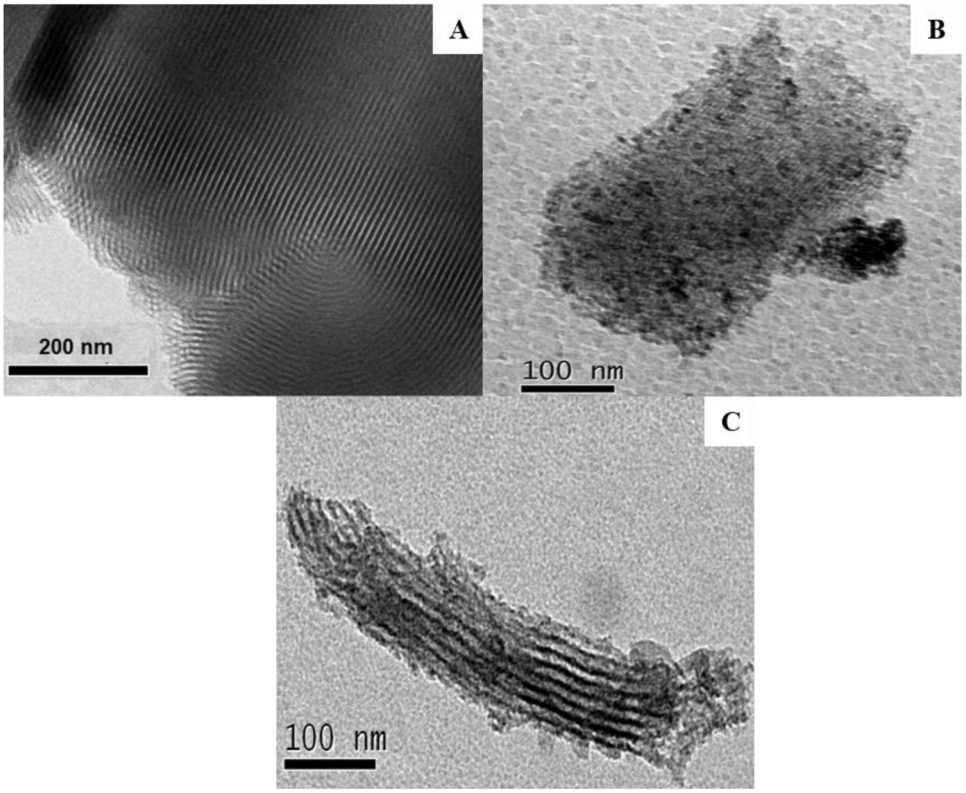

Fig. 4. HRTEM images of pristine SBA-15 (A), 16% TiO_2/SBA-15 (B) and PMONDI-16 (C).

the Scherrer formula as 5.24 nm, which agrees with the TEM image (Fig. 4B).

Fig. S1 shows the diffuse reflectance spectra of the catalysts PMONDI-16% and 16% TiO_2/SBA-15. As noticed, the absorption of the PMONDI catalysts extends into the visible range, until ca. 440 nm, corresponding to a bandgap of 2.8 eV, whereas the absorption of the TiO_2 catalyst vanishes at 400 nm (bandgap of 3.1 eV). Absorption in the visible is a desirable characteristic for a photocatalyst, since it will enhance the absorption of solar light. Also note the greater overlap of the lamp emission with the absorption of PMONDI-16 as compared to the absorption of the TiO_2 catalyst (Fig. S1). The visible absorption tail can be attributed to π-stacking of the NDI units in PMONDI-16, since NDI derivatives in homogeneous solutions do not absorb in the visible (Castanheira et al., 2018).

3.2. Photodegradation of SDZ

Fig. 5 shows the decay of SDZ concentration with time, in the presence of the different photocatalysts, before and after the beginning of irradiation with the Hg lamp, in the conditions that gave the best results. The vertical dashed line represents the time the lamp was turned on. The period in the dark corresponds to SDZ removal by adsorption. It can be observed that the amount of SDZ removed by adsorption was much smaller than the amount removed by photocatalysis, reaching a maximum of only 9%, observed with PMONDI-16.

The PMONDI photocatalysts were clearly more efficient than the TiO_2 based material under these conditions. SDZ was no more identified after 45 min irradiation with PMONDI-16, and after 90 min with PMONDI-8. In contrast, complete SDZ degradation was observed only after ca 150 min with 16% TiO_2/SBA-15. Accordingly, the pseudo first-order specific degradation rate for SDZ (Eq. 2) increased from 3.1×10^{-2} min^{-1} in 16% TiO_2/SBA-15–4.5×10^{-2} min^{-1} in PMONDI-8 and 5.8×10^{-2} min^{-1} in PMONDI-16 (Table S1). Direct photolysis was also observed in these conditions (Fig. S3), which is due to a small overlap of SDZ absorption with the lamp emission (Fig. S1). This effect was more pronounced in the presence of pristine SBA-15, but the extent of SDZ degradation in these cases was much smaller than with the PMONDI and TiO_2 photocatalysts (Fig. 5).

Fig. S3 shows equivalent experiments performed in different conditions of irradiance and initial SDZ concentration. As observed, the PMONDI catalysts were more efficient then the TiO_2 catalyst in most conditions tested, except for the lowest intensity employed (I = 3 mW cm^{-2}).

The photodegradation rate was found to increase with increasing irradiance for all photocatalysts, as expected. The rate constant increased nearly five times in the presence of the PMONDI catalysts and three times in the presence of 16% TiO_2/SBA-15, upon increasing the irradiance from 3 to 13 mW cm^{-2} ($[SDZ]_0$ = 7.5 mg L^{-1} in both cases). Fig. 6 shows the effect of varying $[SDZ]_0$, at constant lamp irradiance (I = 8 mW cm^{-2}), on the rate constant of SDZ degradation. As observed, lower $[SDZ]_0$ values favored photodegradation. Degradation was almost twice as fast when $[SDZ]_0$ was reduced to 5 mg L^{-1}.

3.3. Photocatalyst reutilization

The 16% TiO_2/SBA-15 and PMONDI-16 photocatalysts were also evaluated in reutilization experiments. For this, each material was reused in three different SDZ photodegradation cycles. The conditions selected were the highest initial concentration of SDZ ($[SDZ]_0$ = 12.5 mg L^{-1}) and lower irradiance (I = 3 mW cm^{-2}), since in these conditions there was no pronounced photolysis (Fig. S3B). As seen in Fig. 7, the PMONDI-16 photocatalyst performed better than 16% TiO_2/SBA-15 in the reuse experiments. In the presence of PMONDI-16, 97% of the SDZ was degraded in the first cycle, 78% in the second cycle and 57% in the third. With 16% TiO_2/SBA-15, on the other hand, 81% of the SDZ was degraded in the first cycle, 71% in the second and 43% in the third. Therefore, the TiO_2 based catalyst lost activity faster than the PMONDI based catalyst upon reutilization.

Identification of photodegradation products. Transformation products were elucidated by LC-MS analyses of aliquots collected before irradiation and after 180 min of irradiation, in the presence of 16% TiO_2/SBA-15 and PMONDI-16 catalysts (Fig. S4). The chromatogram before irradiation shows only the peak corresponding to SDZ, with retention time of 6.2 min (Fig. S4A) and m/z = 251, which is assignable to SDZ $[M+H]^+$ (Baran et al., 2006). After irradiation with 16% TiO_2/SBA-15,

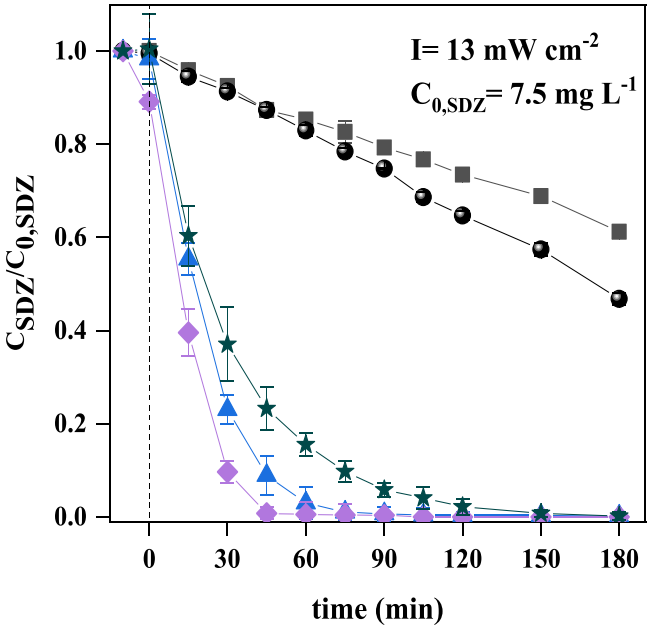

Fig. 5. Decay of [SDZ] in the presence of different photocatalysts: 16% TiO_2/SBA-15 (—★—), PMONDI-8 (—▲—), PMONDI-16 (—◆—) and pristine SBA-15 (—●—). Direct SDZ photolysis is also shown (—■—). The dashed line represents the time the lamp was turned on, after 24 h stirring in the dark.

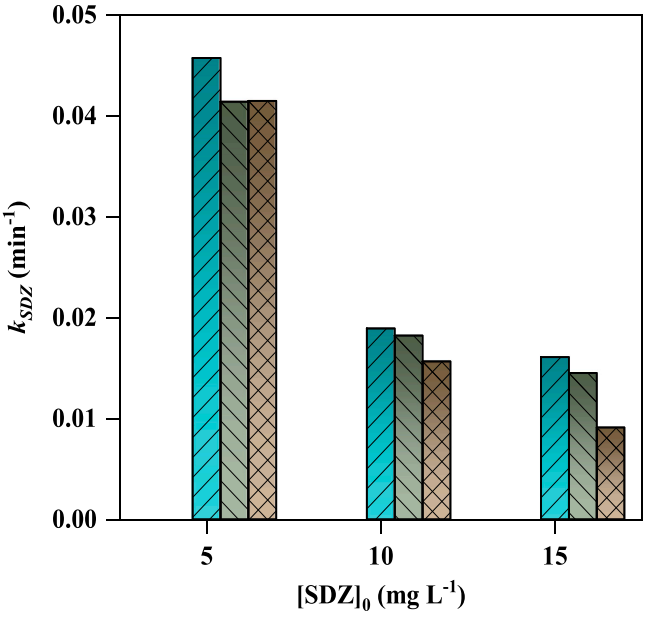

Fig. 6. Effect of initial SDZ concentration on the pseudo-first order rate constants of SDZ photodegradation (I = 8 mW cm^{-2}). PMONDI-8 ( ); PMONDI-16 ( ); 16% TiO_2/SBA-15 ( ).

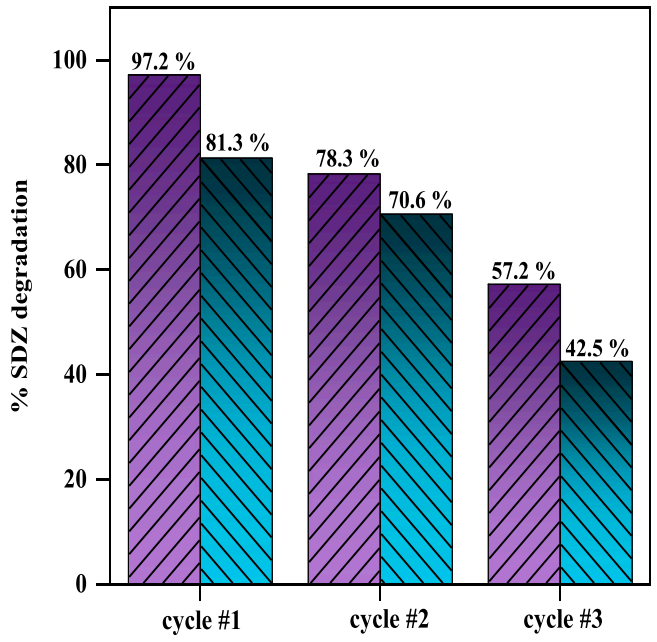

Fig. 7. Extent of SDZ degradation upon reutilization of the catalysts over three photocatalytic cycles. PMONDI-16 ( ); 16% TiO_2/SBA-15 ( ).

82.8% degradation of SDZ was observed, with the appearance of three new peaks, corresponding to degradation products (Fig. S4B). The degradation products could be identified based on their *m/z* ratio (Fig. S4) and by comparison with published data. The peak identified as P1, with retention time of 3.5 min ($m/z = 187$), corresponds to the extrusion of SO_2 followed by rearrangement, forming 4-(2-amino-pyrimidine-1(2 H)-yl)-aniline (Scheme 1). This product has been reported in the literature by several authors (Boreen et al., 2005a, 2005b; McNeill and Canonica, 2016; Batista et al., 2016a, 2014; Ji et al., 2017). Oxidation of the aniline ring in this intermediate to nitrobenzene (Scheme 1) produces the product identified as P2 (retention time: 2.2 min, $m/z = 219$). The peak identified as P3 (retention time: 5.3 min, $m/z = 267$) corresponds to SDZ $[M+H]^+$ with the addition of 16 mass units, indicating hydroxylation of SDZ (Scheme 1). Hydroxylation occurs preferentially in the aniline ring, being less likely in the pyrimidine ring due to its higher electron density (Baran et al., 2006).

Remarkably, irradiation in the presence of PMONDI-16 led to almost complete degradation of SDZ (93.8%) (Fig. S4C). The peak of SDZ was replaced by three new peaks after irradiation, corresponding to P1 and P2, along with a third peak with retention time of 2.8 min and $m/z = 187$. This peak can also be attributed to the product P1, since it has the same *m/z* ratio as the peak with retention time of 3.5 min. Other authors have associated the SO_2 extrusion product to two different retention times (Perisa et al., 2013; Ma et al., 2015).

The absence of the peak P3 after irradiation with PMONDI-16 suggests different sensitization mechanisms for the two catalysts. Hydroxylation is a result of attack by hydroxyl radicals, whereas SO_2 extrusion and oxidation are the products of $^1O_2$ attack (Ji et al., 2017; Boreen et al., 2005b; Batista et al., 2016b). Both processes apparently took place with 16% TiO_2/SBA-15, but only $^1O_2$ attack occurred with PMONDI-16. This finding is in agreement with the generally accepted mechanism for NDI sensitization (Castanheira et al., 2017, 2018; Andrade et al., 2020; Moraes et al., 2018; Bhosale et al., 2021; Aveline et al., 1997; Rogers and Kelly, 1999) which involves intersystem crossing of the singlet excited state of NDI to the triplet state. Triplet NDI readily reacts with molecular oxygen by energy transfer, giving $^1O_2$, as shown in Scheme 2 (Type II mechanism). This route could be confirmed through the $^1O_2$ photoproduction measurements using FFA as a probe compound in the presence of PMONDI-16 catalyst. Fig. S6 shows the decline in FFA concentration, giving $^1O_2$ at a steady state concentration ($[^1O_2]_{SS}$) on the order of 10^{-12} mol L^{-1}, which is in accordance with the literature (Ribeiro et al., 2015). Triplet NDI can also oxidize SDZ directly by electron transfer, giving $NDI^{\bullet-}$ and $SDZ^{\bullet+}$, followed by decomposition of the SDZ radical (Type I mechanism) and the regeneration of NDI by O_2.

4. Conclusions

The immobilization of the organic sensitizer naphthalenediimide within the pore walls of a PMO resulted in a catalyst which efficiently degraded SDZ under UV/visible irradiation. The activity of the PMONDI materials rivals that of standard photocatalysts, such as TiO_2 nanoparticles. The good performance of PMONDI can be attributed to the large, unobstructed pores, as well as the absorption up to 450 nm. In addition, the stability of the PMONDI catalyst was demonstrated by the reuse tests. The present results demonstrate the great potential of PMONDI photocatalysts in the degradation of SDZ, encouraging the evaluation of these materials with other CECs.

CRediT authorship contribution statement

Bruna Castanheira: Conceptualization, Methodology, Validation, Formal analysis, Experimental Investigation, Data curation, Writing – original draft. **Larissa Otubo:** Formal analysis, Data curation, Writing – original draft. **Sergio Brochsztain:** Supervision, Conceptualization, Project administration, Writing – original draft. **Antonio Carlos S. C. Teixeira:** Supervision, Conceptualization, Project administration, Writing – original draft, Resources, Funding acquisition.

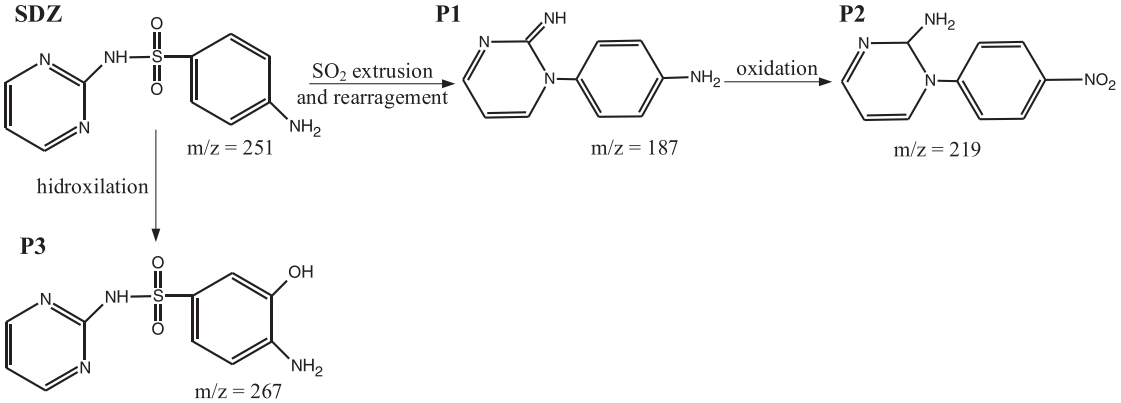

Scheme 1. Observed pathways for SDZ photodegradation.

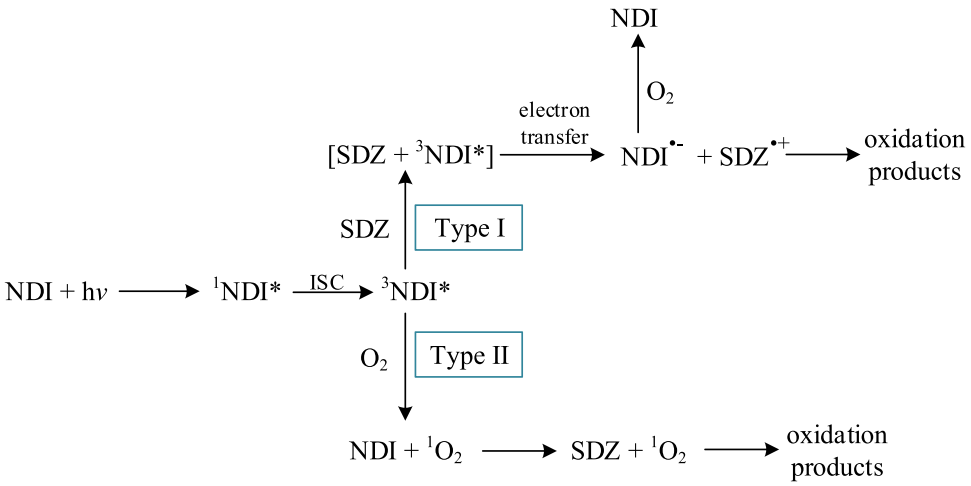

Scheme 2. Proposed mechanism of sensitization by NDI in the photocatalytic degradation of SDZ. ISC: Intersystem crossing.

Declaration of Competing Interest

The authors declare that they have no known competing financial interests or personal relationships that could have appeared to influence the work reported in this paper.

Data Availability

No data was used for the research described in the article.

Acknowledgements

ACSCT acknowledges the São Paulo Research Foundation (FAPESP) (grants #2018/21271–6 and #2019/24158–9) and the National Council for Scientific and Technological Development (CNPq) (grant #311230/2020–2) for the financial support. SB thanks the support of FAPESP (grant #2016/05496–2). The authors thank the Multiuser Central Facilities (UFABC) for the analytical support.

Environmental Implication

Sulfonamide antibiotics are waterborne persistent pollutants. Conventional techniques for the water treatment are not efficient to eliminate such pollutants due to their high chemical stability. In this context, the heterogeneous photocatalysis was investigated for the degradation of sulfadiazine (SDZ). For this, novel photocatalytic materials consisting of periodic mesoporous organosilicas (PMO) functionalized naphthalenediimide (NDI) were used. PMONDI showed a great potential to eliminate the SDZ from the water. Given that, we do believe that the present work constitutes an important contribution to advanced materials/technologies dedicated to the removal of hazardous contaminants, particularly those related to antimicrobial resistance.

Appendix A. Supporting information

Supplementary data associated with this article can be found in the online version at doi:10.1016/j.jhazmat.2022.130224.

References

Acosta-Silva, Y.J., Nava, R., Hernández-Morales, V., Macías-Sánchez, S.A., Gómez-Herrera, M.L., Pawelec, B., 2011. Methylene blue photodegradation over titania-decorated SBA-15. Appl. Catal. B Environ. 110, 108–117.

Ahmed, M.B., Zhou, J.L., Ngo, H.H., Guo, W., Thomaidis, N.S., Xu, J., 2017. Progress in the biological and chemical treatment technologies for emerging contaminant removal from wastewater: acritical review. J. Hazard. Mater. 323, 274–298.

Andrade, L.S., Castanheira, B., Brochsztain, S., 2020. Periodic mesoporous organosilicas containing naphthalenediimides within the pore walls for asphaltene adsorption. Microporous Mesoporous Mater. 294, 109909.

Aveline, B.M., Matsugo, S., Redmond, R.W., 1997. Photochemical mechanisms responsible for the versatile application of naphthalimides and naphthaldiimides in biological systems. J. Am. Chem. Soc. 119, 11785–11795.

Baran, W., Sochacka, J., Wardas, W., 2006. Toxicity and biodegradability of sulfonamides and products of their photocatalytic degradation in aqueous solutions. Chemosphere 65, 1295–1299.

Baran, W., Adamek, E., Ziemiańska, J., Sobczak, A., 2011. Effects of the presence of sulfonamides in the environment and their influence on human health. J. Hazard. Mater. 196, 1–15.

Batista, A.P.S., Pires, F.C.C., Teixeira, A.C.S.C., 2014. Photochemical degradation of sulfadiazine, sulfamerazine and sulfamethazine: relevance of concentration and heterocyclic aromatic groups to degradation kinetics. J. Photochem. Photobiol. A: Chem. 286, 40–46.

Batista, A.P.S., Teixeira, A.C.S.C., Cooper, W.J., Cottrell, B.A., 2016a. Correlating the chemical and spectroscopic characteristics of natural organic matter with the photodegradation of sulfamerazine. Water Res 93, 20–29.

Batista, A.P.S., Teixeira, A.C.S.C., Cooper, W.J., Cottrell, B.A., 2016b. Correlating the chemical and spectroscopic characteristics of natural organic matter with the photodegradation of sulfamerazine. Water Res. 93, 20–29.

Bhosale, S.V., Al Kobaisi, M., Jadhav, R.W., Morajkar, P.P., Jones, L.A., George, S., 2021. Naphthalene diimides: perspectives and promise. Chem. Soc. Rev. 50, 9845–9998.

Boreen, A.L., Arnold, W.A., McNeill, K., 2005a. Triplet-sensitized photodegradation of sulfa drugs containing six-membered heterocyclic groups: identification of an SO_2 extrusion photoproduct. Environ. Sci. Technol. 39, 3630–3638.

Boreen, A.L., Arnold, W.A., McNeill, K., 2005b. Triplet-sensitized photodegradation of sulfa drugs containing six-membered heterocyclic groups: identification of an SO_2 extrusion photoproduct. Environ. Sci. Technol. 39, 3630–3638.

Castanheira, B., Trindade, F.J., Andrade, L.S., Nantes, I.L., Politi, M.J., Triboni, E.R., Brochsztain, S., 2017. Dye photodegradation employing mesoporous organosilicas functionalized with 1,8-naphthalimides as heterogeneous catalysts. J. Photochem. Photobiol. A: Chem. 332, 316–325.

Castanheira, B., Triboni, E.R., Andrade, L.S., Trindade, F.J., Otubo, L., Teixeira, A.C., Politi, M.J., Queiroz, T.B., Brochsztain, S., 2018. Synthesis of novel periodic mesoporous organosilicas containing 1,4,5,8-Naphthalenediimides within the pore walls and their reduction to generate wall-embedded free radicals. Langmuir 34, 8195–8204.

Castanheira, B., Otubo, L., Oliveira, C.L.P., Montes, R., Quintana, J.B., Rodil, R., Brochsztain, S., Vilar, V.J.P., Teixeira, A.C.S.C., 2022. Functionalized mesoporous silicas SBA-15 for heterogeneous photocatalysis towards CECs removal from secondary urban wastewater. Chemosphere 287, 132023.

Chongdar, S., Bhattacharjee, S., Bhanja, P., Bhaumik, A., 2022. Porous organic–inorganic hybrid materials for catalysis, energy and environmental applications. Chem. Commun. 58, 3429–3460.

Conceição, D.S., Graça, C.A.L., Ferreira, D.P., Ferraria, A.M., Fonseca, I.M., do Rego, A. M.B., Teixeira, A.C.S.C., Ferreira, L.F.V., 2017. Photochemical insights of TiO_2 decorated mesoporous SBA-15 materials and their influence on the photodegradation of organic contaminants. Microporous Mesoporous Mater. 253, 203–214.

Deka, J.R., Liu, C.-L., Wang, T.-H., Chang, W.-C., Kao, H.-M., 2014. Synthesis of highly phosphonic acid functionalized benzene-bridged periodic mesoporous organosilicas for use as efficient dye adsorbents. J. Hazard. Mater. 278, 539–550.

Esquivel, D., Ouwehand, J., Meledina, M., Turner, S., Tendeloo, G.V., Romero-Salguero, F.J., De Clercq, J., Van Der Voort, P., 2017. Thiol-ethylene bridged PMO: A high capacity regenerable mercury adsorbent via intrapore mercury thiolate crystal formation. J. Hazard. Mater. 339, 368–377.

Fagan, R., McCormack, D.E., Dionysiou, D.D., Pillai, S.C., 2016. A review of solar and visible light active TiO_2 photocatalysis for treating bacteria, cyanotoxins and contaminants of emerging concern. Mater. Sci. Semicond. Process. 42, 2–14.
Hoffmann, F., Cornelius, M., Morell, J., Fröba, M., 2006. Silica-based mesoporous organic–inorganic hybrid materials. Angew. Chem. Int. Ed. 45, 3216–3251.
Ji, Y., Shi, Y., Wang, L., Lu, J., Ferronato, C., Chovelon, J.-M., 2017. Sulfate radical-based oxidation of antibiotics sulfamethazine, sulfapyridine, sulfadiazine, sulfadimethoxine, and sulfachloropyridazine: formation of SO_2 extrusion products and effects of natural organic matter. Sci. Total Environ. 593- 594, 704–712.
Karimi, B., Ganji, N., Pourshiani, O., Thiel, W.R., 2022. Periodic mesoporous organosilicas (PMOs): From synthesis strategies to applications. Prog. Mater. Sci. 125, 100896.
Kovalakova, P., Cizmas, L., McDonald, T.J., Marsalek, B., Feng, M., Sharma, V.K., 2020. Occurrence and toxicity of antibiotics in the aquatic environment: a review. Chemosphere 251, 126351.
Krzeminski, P., Tomei, M.C., Karaolia, P., Langenhoff, A., Almeida, C.M.R., Felis, E., Gritten, F., Andersen, H.R., Fernandes, T., Manaia, C.M., Rizzo, L., Fatta-Kassinos, D., 2019. Performance of secondary wastewater treatment methods for the removal of contaminants of emerging concern implicated in crop uptake and antibiotic resistance spread: a review. Sci. Total Environ. 648, 1052–1081.
Kumar, S., Shukla, J., Kumar, Y., Mukhopadhyay, P., 2018. Electron-poor arylenediimides. Org. Chem. Front. 5, 2254–2276.
Kümmerer, K., 2009a. Antibiotics in the aquatic environment – a review – Part I. Chemosphere 75, 417–434.
Kümmerer, K., 2009b. Antibiotics in the aquatic environment – a review – Part II. Chemosphere 75, 435–441.
Lee, B.C.Y., Lim, F.Y., Loh, W.H., Ong, S.L., Hu, J., 2021. Emerging contaminants: an overview of recent trends for their treatment and management using light-driven processes. Water 13, 2340.
Lopez-Munoz, M.-J., van Grieken, R., Aguado, J., Marugan, J., 2005. Role of the support on the activity of silica-supported TiO_2 photocatalysts: structure of the TiO_2/SBA-15 photocatalysts. Catal. Today 101, 307–314.
Ma, Y., Zhang, K., Li, C., Zhang, T., Gao, N., 2015. Oxidation of sulfonamides in aqueous solution by UV-TiO_2-Fe(VI). BioMed. Res. Int., 973942
McNeill, K., Canonica, S., 2016. Triplet state dissolved organic matter in aquatic photochemistry: reaction mechanisms, substrate scope, and photophysical properties. Environ. Sci.: Process. Impacts 18, 1381–1399.
Miklos, D.B., Remy, C., Jekel, M., Linden, K.G., Drewes, J.E., Hübner, U., 2018. Evaluation of advanced oxidation processes for water and wastewater treatment – a critical review. Water Res. 139, 118–131.
Miranda-García, N., Suárez, S., Maldonado, M.I., Malato, S., Sánchez, B., 2014. Regeneration approaches for TiO_2 immobilized photocatalyst used in the elimination of emerging contaminants in water. Catal. Today 230, 27–34.
Mizoshita, N., Tani, T., Inagaki, S., 2011. Syntheses, properties and applications of periodic mesoporous organosilicas prepared from bridged organosilane precursors. Chem. Soc. Rev. 40, 789–800.
Moraes, T.B.F., Schimidt, M.F.R.A., Bacani, R., Weber, G., Politi, M.J., Castanheira, B., Brochsztain, S., Silva, F.A., Demets, G.J.F., Triboni, E.R., 2018. Polysilsesquioxane naphthalenediimide thermo and photochromic gels. J. Lumin. 204, 685–691.
Mostafa, S., Rosario-Ortiz, F.L., 2013. Singlet oxygen formation from wastewater organic matter. Environ. Sci. Technol. 47 (15), 8179–8186.
Parida, V.K., Saidulu, D., Majumder, A., Srivastava, A., Gupta, B., Gupta, A.K., 2021. Emerging contaminants in wastewater: a critical review on occurrence, existing legislations, risk assessment, and sustainable treatment alternatives. J. Environ. Chem. Eng. 9, 105966.
Park, S.S., Moorthy, M.S., Ha, C.-S., 2014. Periodic mesoporous organosilicas for advanced applications. NPG Asia Mater. 6, e96.
Perisa, M., Babic, S., Škorić, I., Frömel, T., Knepper, T.P., 2013. Photodegradation of sulfonamides and their N^4-acetylated metabolites in water by simulated sunlight irradiation: kinetics and identification of photoproducts. Environ. Sci. Pollut. Res. 20, 8934–8946.
Ribeiro, A.R., Nunes, O.C., Pereira, M.F.R., Silva, A.M.T., 2015. An overview on the advanced oxidation processes applied for the treatment of water pollutants defined in the recently launched Directive 2013/39/EU. Environ. Int. 75, 33–51.
Rivas-Ortiz, I.B., Cruz-González, G., Lastre-Acosta, A.M., Manduca-Artiles, M., Rapado-Paneque, M., Chávez-Ardanza, A., Teixeira, A.C.S.C., Jáuregui-Haza, U.J., 2017. Optimization of radiolytic degradation of sulfadiazine by combining Fenton and gamma irradiation processes. J. Radioanal. Nucl. Chem. 314, 2597–2607.
Rivera-Utrilla, J., Sánchez-Polo, M., Ferro-García, M.A., Prados-Joya, G., Ocampo-Pérez, R., 2013. Pharmaceuticals as emerging contaminants and their removal from water. A review. Chemosphere 93, 1268–1287.
Rizzo, L., Malato, S., Antakyali, D., Beretsou, V.G., Đolić, M.B., Gernjak, W., Heath, E., Ivancev-Tumbas, I., Karaolia, P., Ribeiro, A.R.L., Mascolo, G., McArdell, C.S., Schaar, H., Silva, A.M.T., Fatta-Kassinos, D., 2019. Consolidated vs new advanced treatment methods for the removal of contaminants of emerging concern from urban wastewater. Sci. Total Environ. 655, 986–1008.
Rodriguez-Narvaez, O.M., Peralta-Hernandez, J.M., Goonetilleke, A., Bandala, E.R., 2017. Treatment technologies for emerging contaminants in water: a review. Chem. Eng. J. 323, 361–380.
Rogers, J.E., Kelly, L.A., 1999. Nucleic acid oxidation mediated by naphthalene and benzophenone imide and diimide derivatives: consequences for DNA redox chemistry. J. Am. Chem. Soc. 121, 3854–3861.
Salameh, C., Nogier, J.-P., Launay, F., Boutros, M., 2015. Dispersion of colloidal TiO_2 nanoparticles on mesoporous materials targeting photocatalysis applications. Catal. Today 257, 35–40.
Tijani, J.O., Fatoba, O.O., Babajide, O.O., Petrik, L.F., 2016. Pharmaceuticals, endocrine disruptors, personal care products, nanomaterials and perfluorinated pollutants: a review. Environ. Chem. Lett. 14, 27–49.
Van Der Voort, P., Esquivel, D., De Canck, E., Goethals, F., Van Driessche, I., Romero-Salguero, F.J., 2013. Periodic mesoporous organosilicas: from simple to complex bridges; a comprehensive overview of functions, morphologies and applications. Chem. Soc. Rev. 42, 3913–3955.
Yang, J., Zhang, J., Zhu, L., Chen, S., Zhang, Y., Tang, Y., Zhu, Y., Li, Y., 2006. Synthesis of nano titania particles embedded in mesoporous SBA-15: characterization and photocatalytic activity. J. Hazard. Mater. B 137, 952–958.
Yang, J., Li, Z., Zhu, H., 2017. Adsorption and photocatalytic degradation of sulfamethoxazole by a novel composite hydrogel with visible light irradiation. Appl. Catal. B: Environ. 217, 603–614.
Zessel, K., Mohring, S., Hamscher, G., Kietzmann, M., Stahl, J., 2014. Biocompatibility and antibacterial activity of photolytic products of sulfonamides. Chemosphere 100, 167–174.
Zhao, D., Huo, Q., Feng, J., Chmelka, B.F., Stucky, G.D., 1998. Nonionic triblock and star diblock copolymer and oligomeric surfactant syntheses of highly ordered, hydrothermally stable, mesoporous silica structures. J. Am. Chem. Soc. 120, 6024–6036.